Monthly Notices
of the
ROYAL ASTRONOMICAL SOCIETY

MNRAS **448,** 1687–1703 (2015) doi:10.1093/mnras/stv026

Isolating the pre-main sequence in Collinder 34, NGC 3293, NGC 3766 and NGC 6231

T. A. Saurin,* E. Bica and C. Bonatto

Departamento de Astronomia, Universidade Federal do Rio Grande do Sul, CP 15051, RS, Porto Alegre 91501-970, Brazil

Accepted 2015 January 6. Received 2014 December 18; in original form 2014 July 17

ABSTRACT

We employed field star decontaminated Two Micron All Sky Survey photometry to study four nearby optical embedded clusters – Collinder 34, NGC 3293, NGC 3766 and NGC 6231 – obtaining deep colour–magnitude diagrams and stellar radial density profiles. We found what seem to be pre-main sequences detached in different amounts from main sequences in these diagrams. The structural analysis of each cluster revealed different radial distributions for these two sequences. We argued that the detached evolutionary sequences in our sample may be evidence of sequential star formation. Finally, we compared the sample cluster parameters with those of other young clusters in the literature and point out evidence that NGC 3766 and NGC 6231 might be evolving to OB associations.

Key words: open clusters and associations: individual: Collinder 34 – open clusters and associations: individual: NGC 3293 – open clusters and associations: individual: NGC 3766 – open clusters and associations: individual: NGC 6231.

1 INTRODUCTION

Young star clusters remain embedded in molecular clouds during the first ∼10 Myr of their existence, so that their stellar content should be observed in infrared wavelengths (Lada & Lada 2003). During this stage, they have a lot of stars that do not fuse hydrogen yet, the pre-main sequence (PMS) stars distinguished from the main-sequence (MS) stars.

As plotted in a colour–magnitude diagram (CMD), these two classes of stars are distributed along different tracks that can be modelled by means of theoretical isochrones (e.g. Siess, Dufour & Forestini 2000; Marigo et al. 2008). Stars with colour and magnitudes occurring along the same curve are expected to be coeval. Factors such as binarity, variability, differential reddening, photometric uncertainties and continuous star formation cause spread around these isochrones (Bonatto, Bica & Lima 2012a,b). Photometry of PMS stars is specially affected by these factors. Among them stand out the T Tauri, young variables with circumstellar discs and infrared excess emission (Furlan et al. 2009).

Snapshots of the dynamical stages of a star cluster may be obtained from radial density profiles (RDPs). Embedded clusters are not expected to have profiles following an isothermal sphere model (e.g. King 1962). Nevertheless, some of these density profiles are fitted by a King-like model providing reliable structural parameters. RDP analyses can also reveal clues on cluster dissolution when extended profiles are observed (e.g. Saurin, Bica & Bonatto 2012) and gradients in the ratios of high-to-low-mass and old-to-young stars that may be interpreted as mass and age segregation (e.g. Hillenbrand 1997).

Using Two Micron All Sky Survey (2MASS;[1] Skrutskie et al. 2006) photometry we analyse the evolutionary sequences and radial profiles of a sample of young clusters in order to investigate triggered/sequential star formation (e.g. Saurin, Bica & Bonatto 2010). The sample consists of objects catalogued by Collinder (1931) who has established some of the bases of the modern cluster analysis. We selected four clusters, the little studied Collinder 34, plus NGC 3293 (Collinder 224), NGC 3766 (Collinder 248) and NGC 6231 (Collinder 315) that are bright nearby young clusters previously studied in various wavelengths (e.g. Dias et al. 2002; Kharchenko et al. 2013). In this work, we perform a field star decontamination procedure in order to isolate and go deeper than previous studies into the PMS of these clusters.

This paper is organized as follows. In Section 2, we explain the field star decontamination method. In Section 3, we build CMDs and estimate astrophysical parameters. In Section 4, we analyse the RDPs and derive structural parameters. In Section 5, we discuss the results. Finally, in Section 6 we give the concluding remarks.

2 2MASS PHOTOMETRY AND FIELD STAR DECONTAMINATION

We used the catalogue II/246 (Cutri et al. 2003) available in the VizieR[2] data base (Ochsenbein, Bauer & Marcout 2000) to extract

* E-mail: tiago.saurin@ufrgs.br

[1] http://www.ipac.caltech.edu/2mass
[2] http://vizier.u-strasbg.fr/viz-bin/VizieR

Table 1. Adopted central coordinates for the clusters. By columns: (1) star cluster identification; (2) Galactic longitude; (3) Galactic latitude; (4) right ascension (J2000); (5) declination (J2000).

Cluster (1)	l (2)	b (3)	α (4)	δ (5)
Collinder 34	138.°03	+1.°50	$02^h59^m23\overset{s}{.}17$	$+60°33'59\overset{''}{.}5$
NGC 3293	285.°86	+0.°07	$10^h35^m53\overset{s}{.}10$	$-58°13'55\overset{''}{.}5$
NGC 3766	294.°12	−0.°03	$11^h36^m14\overset{s}{.}00$	$-61°36'30\overset{''}{.}0$
NGC 6231	343.°46	+1.°18	$16^h54^m10\overset{s}{.}06$	$-41°49'30\overset{''}{.}1$

the 2MASS photometry of the clusters in the J, H and K_S bands within large circular areas ($r = 100$ arcmin). We restricted our analyses to stars with photometric errors $\leq$0.1 mag in each band.

The cluster coordinates in WEBDA[3] were taken as the starting point to find an optimized centre, which corresponds to the RDP with the highest stellar density at the innermost (radial) bin (Table 1). We found that Collinder 34 was better centred on its brightest star, HD 18326; for NGC 3293, we chose the centre near the Be star V439 Car; for NGC 3766, the WEBDA coordinates were kept. Finally, for NGC 6231, the coordinates of the eclipsing binary star V1007 Sco proved to be adequate.

Field star contamination is expected to be present in essentially all cluster observations, especially when the object is close to the Galactic plane. Therefore, it is necessary to isolate the probable cluster members. We use a method that performs a comparison between the photometric properties of the stars in an offset field and the cluster area (e.g. Bonatto & Bica 2007; Bonatto & Bica 2010). It works according to the following algorithm.

(i) A circular area of radius 10 arcmin (or 20 arcmin) of the cluster and an annular area ($80 \leq r \leq 100$ arcmin) of the field were selected. The contamination in the cluster area was modelled by comparison of three-dimensional CMDs $J \times (J-H) \times (J-K_S)$ of both regions. These CMDs were divided by cells of dimensions $\Delta J = 1.0$ and $\Delta(J-H) = \Delta(J-K_S) = 0.2$, where the probability of a star to be member was computed. Thus, the density of stars was obtained in each cell of the cluster and field CMDs.

(ii) The comparison field density was converted into an integer number of stars to be subtracted from that in the cluster area, on a cell-by-cell basis, resulting the number of member stars in each cell ($N^{\rm cell}_{\rm clean}$). Shifts in the cell positioning corresponding to 1/3 of the adopted cell size in each dimension were allowed, so that 243 different setups were run, each one with a total number of member stars $N_{\rm mem} = \sum_{\rm cell} N^{\rm cell}_{\rm clean}$. By averaging these values, the expected number of member stars was computed within the extraction area of the cluster ($\langle N_{\rm mem}\rangle$).

(iii) The $\langle N_{\rm mem}\rangle$ stars that have more often survived the 243 runs were considered cluster members and transposed to the decontaminated CMD. The difference between the expected number of field stars (sometimes fractional) and the number of stars effectively subtracted (integer) from each cell provides the subtraction efficiency.

The resulting subtraction efficiencies were 90.4 ± 1.8 per cent for Collinder 34, 83.4 ± 1.0 per cent for NGC 3293, 92.5 ± 0.5 per cent for NGC 3766, and 82.8 ± 0.9 per cent for NGC 6231.

We emphasize that the clean CMDs are essential guides for the optimal setting of theoretical isochrone curves and estimating reliable parameters (Section 3). Circular areas of different radii were tested, but we found that larger radii resulted in lower subtraction efficiencies, while smaller radii removed too many points from the CMDs – including stars catalogued as members.

3 COLOUR–MAGNITUDE DIAGRAMS

In Figs 1–4 are shown the 2MASS CMD $J \times (J-H)$ and $J \times (J-K_S)$ of the four clusters. The CMDs present raw cluster photometry within the circular areas (Section 2), field star photometry within an annulus of equal area, and cluster decontaminated photometry.

The decontamination procedure enhances the PMS and enables to detect the low-mass limit of the MS, as expected from PMS to MS evolution. This cutoff is detected for all sample clusters (Figs 1–4). An important feature in the CMDs of the sample is the colour separation between the MS and probable PMS. This feature has also been observed in Trumpler 37 (Saurin et al. 2012).

2MASS photometric uncertainties and degeneracies do not allow us to detect metallicity differences for young populations. Thus, we adopted Solar-metallicity isochrones, suitable for the Galactic disc in general. For the MS of all clusters, we used 10 or 20 Myr Padova isochrones (Marigo et al. 2008) plus 0.2, 1 and 5 Myr PMS isochrones of Siess et al. (2000) converted to 2MASS photometry (Kenyon & Hartmann 1995).

For each cluster, reddening and distance have been obtained by means of a spectral type calibration using a catalogued blue star, avoiding spectroscopic binaries and variables (Table 2). The following stars listed in the SIMBAD[4] astronomical data base (Wenger et al. 2000) have been used in spectral type calibrations: TYC 4048-1432-1 for Collinder 34, CPD-57 3520 for NGC 3293, CPD-60 3120 for NGC 3766, and SBL 164 for NGC 6231. Table 3 shows the parameters $(m-M)J$, $E(J-H)$ and $E(J-K_S)$, obtained from the MS isochrone solutions, and $E(H-K_S)$, A_J, $E(B-V)$ and A_V, estimated using the relations given by Dutra, Santiago & Bica (2002).

Heliocentric and Galactocentric distances for each cluster have been estimated using the photometric parameters and assuming that the distance from the Sun to the Galactic Centre is $R_\odot = 8.4 \pm 0.6$ kpc (Reid et al. 2009). The resulting values are in Table 4.

A mass estimate of the MS stellar content was made by summing the individual masses of each star according to the mass–luminosity relation for dereddened colours and magnitudes. Collinder 34 has MS stellar masses in the range 1.4–17.8 $M_\odot$, and its MS mass amounts to 359^{+37}_{-27} $M_\odot$. For NGC 3293, the range is 1.7–17.8 $M_\odot$, yielding a MS mass of 899^{+11}_{-8} $M_\odot$. For NGC 3766, the range is 1.2–11.2 $M_\odot$, yielding a MS mass of 1682 ± 31 $M_\odot$. For NGC 6231, the range is 2.5–17.8 $M_\odot$, yielding a MS mass of 1939^{+17}_{-13} $M_\odot$. A similar procedure is not possible for the PMS, so we simply counted the number of stars and multiplied it by a mean PMS stellar mass. This is 0.6 $M_\odot$ by assuming an initial mass function of Kroupa (2001) in the range 0.08–7 $M_\odot$. All these masses were derived within circular areas of radius 10 or 20 arcmin (Section 2) and are summarized in Table 4. Note that these values must be lower limits, owing to the presence of dust and gas, unresolved binaries, and the fact that we have considered only the more probable cluster members (decontaminated CMDs).

Additional comparisons with sequences of dwarfs and giants (Schmidt-Kaler 1982), and the classical T Tauri stars (CTTSs) locus (Meyer, Calvet & Hillenbrand 1997) – transformed into the 2MASS photometric system using the relations derived by Carpenter (2001)

[3] http://webda.physics.muni.cz

[4] http://simbad.u-strasbg.fr/simbad

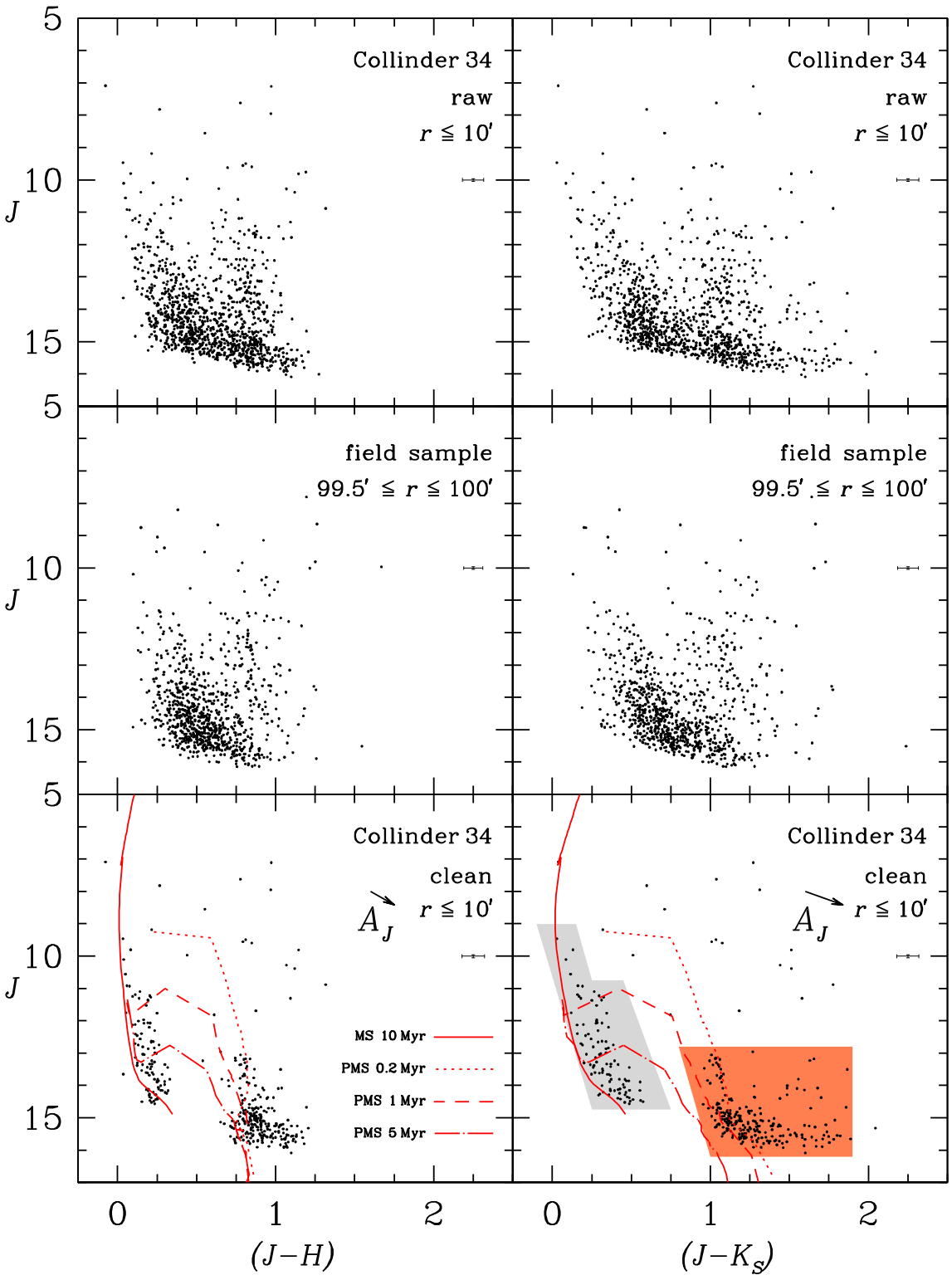

Figure 1. Collinder 34: 2MASS CMD extracted inside $r \leq 10$ arcmin. Mean uncertainties are represented by error bars. Top panels: observed photometry with $J \times (J - H$, left) and $J \times (J - K_S$, right). Middle: field equal-area extraction. Bottom: decontaminated CMDs with 10 Myr Solar-metallicity Padova isochrone and 0.2, 1 and 5 Myr PMS isochrones. Light-shaded polygon: MS colour–magnitude filter. Heavy-shaded polygon: the same for the PMS stars. The arrows indicate the reddening vectors for $A_J = 0.42$ mag.

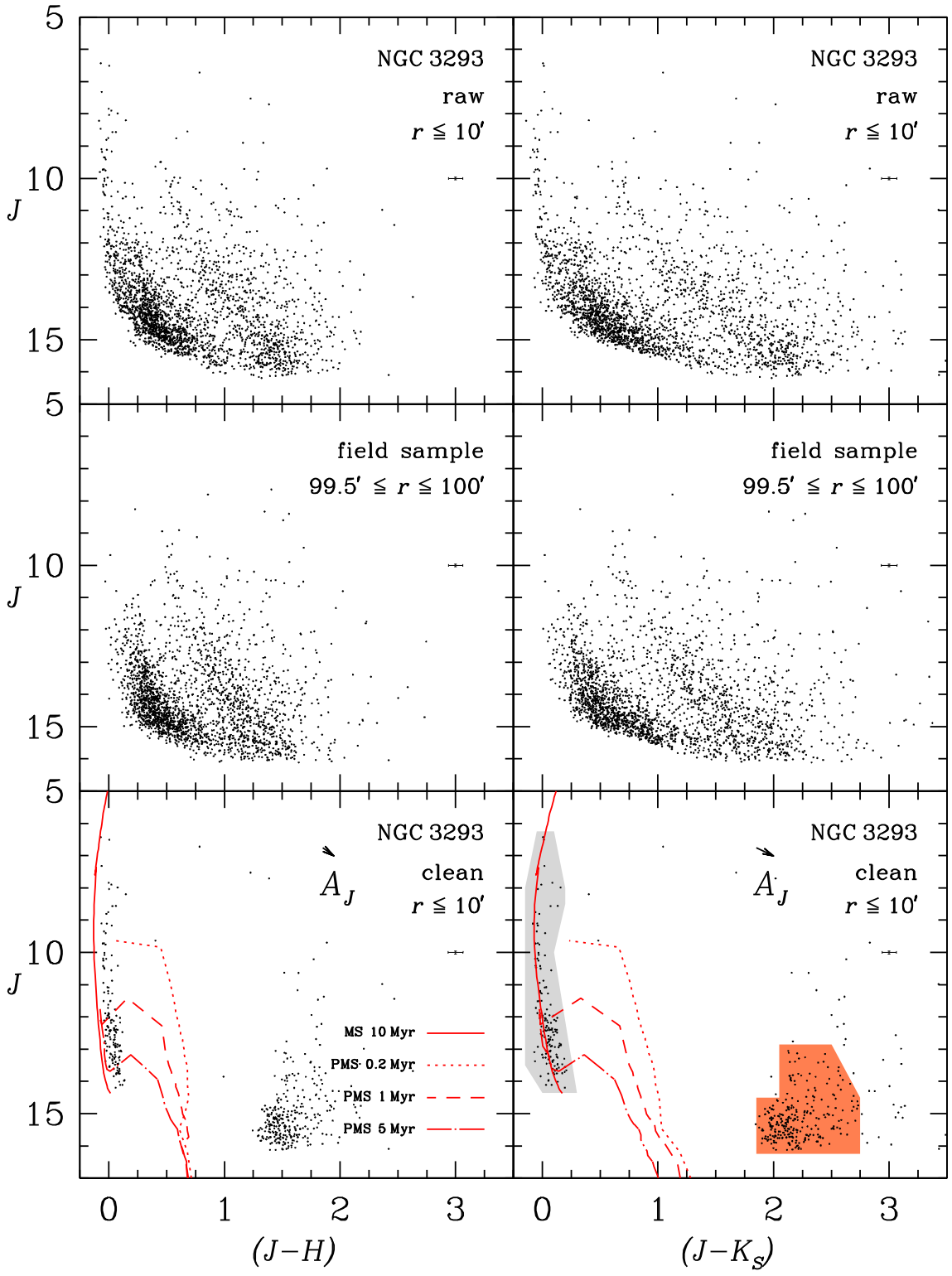

Figure 2. NGC 3293: similar to Fig. 1. The arrows indicate the reddening vectors for $A_J = 0.26$ mag.

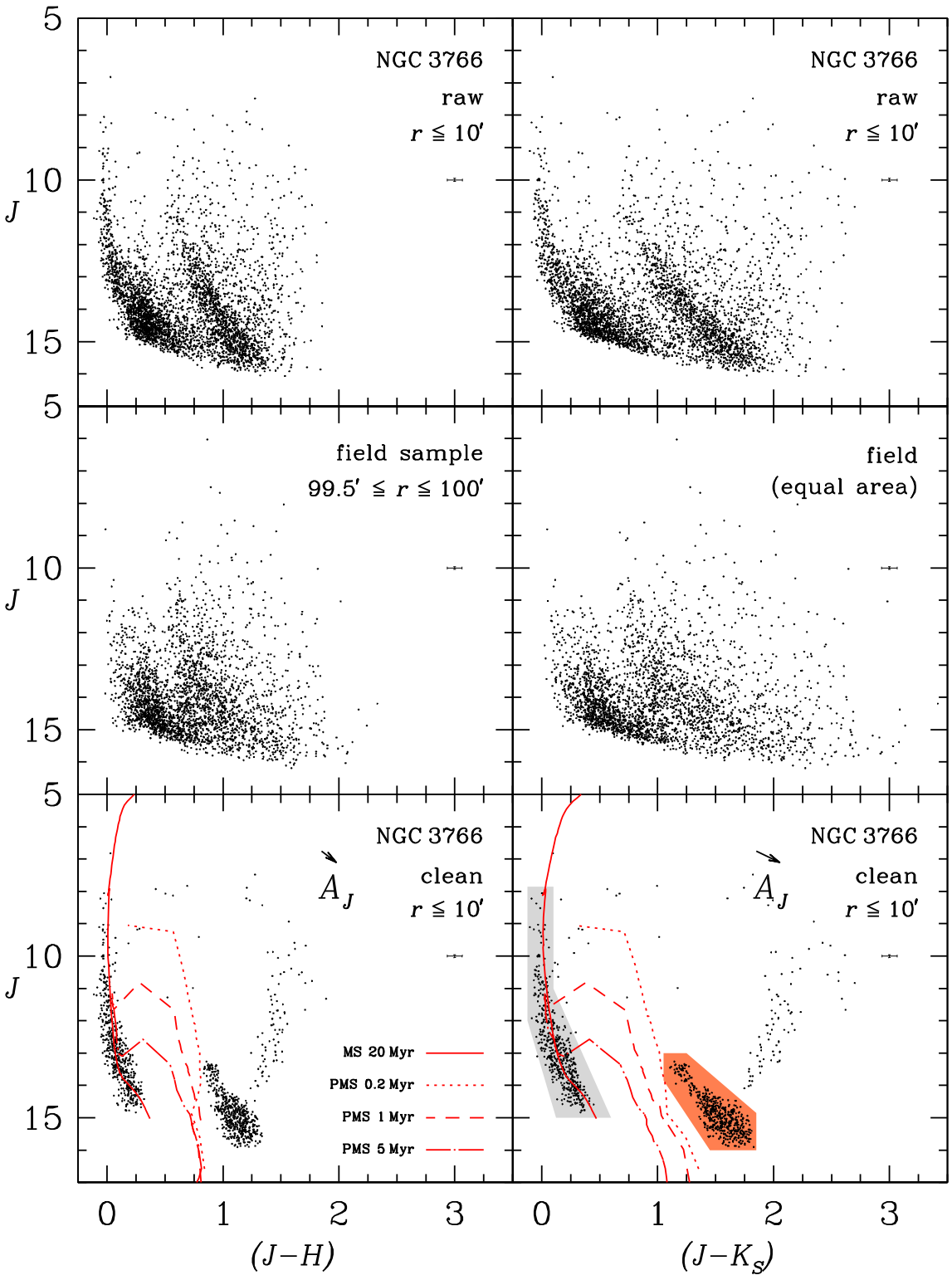

Figure 3. NGC 3766: similar to Fig. 1, but with a 20 Myr Padova isochrone. The arrows indicate the reddening vectors for $A_J = 0.35$ mag.

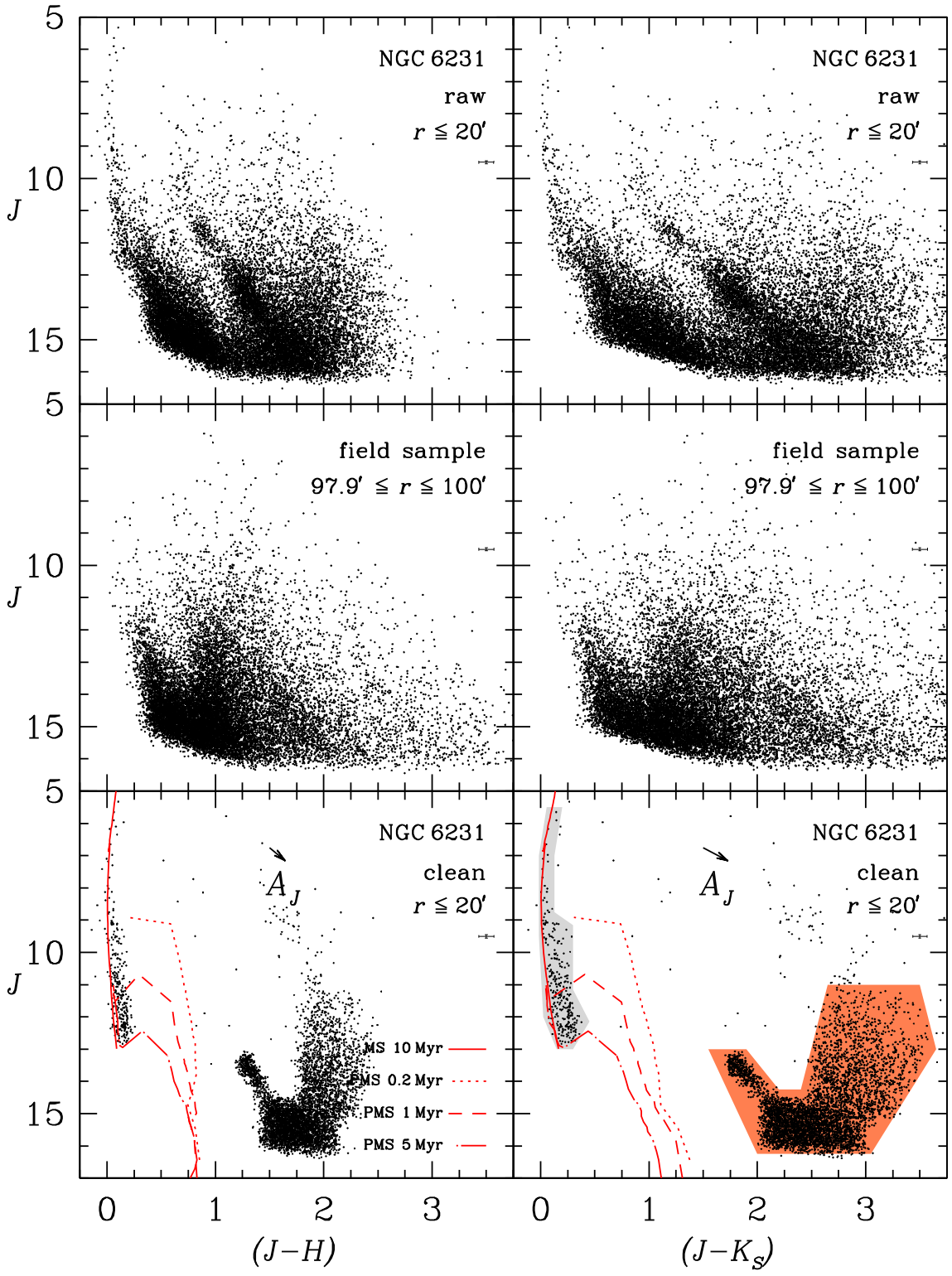

Figure 4. NGC 6231: similar to Fig. 1. The arrows indicate the reddening vectors for $A_J = 0.40$ mag.

Table 2. Reference stars used for the spectral type calibration of the theoretical isochrones. By columns: (1) star identification; (2) associated cluster; (3) right ascension (J2000); (4) declination (J2000); (5) J-band apparent magnitude; (6) $J - H$ colour; (7) $J - K_S$ colour; (8) spectral type.

Star (1)	Cluster (2)	α (3)	δ (4)	m_J (5)	$J - H$ (6)	$J - K_S$ (7)	ST (8)
TYC 4048-1432-1	Collinder 34	$02^h59^m21^s.19$	$+60°25'22''.0$	9.464 ± 0.022	0.034 ± 0.036	0.029 ± 0.030	B8
CPD-57 3520	NGC 3293	$10^h35^m56^s.61$	$-58°12'40''.9$	10.197 ± 0.027	-0.022 ± 0.037	-0.061 ± 0.035	B2
CPD-60 3120	NGC 3766	$11^h36^m08^s.25$	$-61°34'19''.4$	10.661 ± 0.026	0.005 ± 0.037	0.031 ± 0.033	B4
SBL 164	NGC 6231	$16^h53^m46^s.99$	$-41°48'55''.0$	11.683 ± 0.023	0.058 ± 0.038	0.036 ± 0.045	B7

Table 3. Photometric parameters of each cluster. By columns: (1) star cluster identification; (2) distance modulus; (3),(4),(5) 2MASS colour excesses; (6) J-band absorption; (7) $E(B - V)$ colour excess; (8) V-band absorption.

Cluster (1)	$(m - M)J$ (2)	$E(J - H)$ (3)	$E(J - K_S)$ (4)	$E(H - K_S)$ (5)	A_J (6)	$E(B - V)$ (7)	A_V (8)
Collinder 34	12.03 ± 0.19	0.15 ± 0.03	0.24 ± 0.05	0.09 ± 0.02	0.42 ± 0.08	0.49 ± 0.10	1.51 ± 0.30
NGC 3293	12.44 ± 0.03	0.10 ± 0.04	0.15 ± 0.06	0.06 ± 0.02	0.26 ± 0.10	0.31 ± 0.12	0.96 ± 0.37
NGC 3766	11.85 ± 0.03	0.13 ± 0.05	0.20 ± 0.08	0.07 ± 0.03	0.35 ± 0.14	0.41 ± 0.16	1.28 ± 0.50
NGC 6231	11.71 ± 0.02	0.14 ± 0.04	0.23 ± 0.06	0.08 ± 0.02	0.40 ± 0.11	0.46 ± 0.13	1.44 ± 0.40

Table 4. Derived scale parameters and mass of the clusters. By columns: (1) star cluster identification; (2) Heliocentric distance; (3) Galactocentric distance considering $R_\odot = 8.4 \pm 0.6$ kpc; (4) angular radial limit; (5) linear radial limit; (6) MS stellar mass; (7) PMS stellar mass; (8) total stellar mass; (9) age of the MS isochrone.

Cluster (1)	$d_\odot$ (kpc) (2)	d_{GC} (kpc) (3)	r_{RDP} (arcmin) (4)	R_{RDP} (pc) (5)	M_{MS} ($M_\odot$) (6)	M_{PMS} ($M_\odot$) (7)	M ($M_\odot$) (8)	t_{MS} (Myr) (9)
Collinder 34	2.1 ± 0.2	10.1 ± 0.2	15.12 ± 0.70	9.2 ± 1.0	359^{+37}_{-27}	131	490^{+37}_{-27}	10
NGC 3293	2.7 ± 0.1	8.1 ± 0.1	11.77 ± 0.49	9.3 ± 0.6	899^{+11}_{-8}	–	–	10
NGC 3766	2.0 ± 0.1	7.8 ± 0.1	46.27 ± 1.56	26.7 ± 1.9	1682 ± 31	317	1998 ± 31	20
NGC 6231	1.8 ± 0.1	6.7 ± 0.1	68.26 ± 2.41	36.2 ± 2.3	1939^{+17}_{-13}	–	–	10

– in extinction corrected colour–colour diagrams (2CDs) show a significant population in the PMS locus (Figs 5–8).

4 RADIAL DENSITY PROFILES

In order to build a stellar RDP of each cluster over its whole extension (beyond 10 or 20 arcmin) with minimum contamination, we defined colour–magnitude filters (shaded areas in the decontaminated CMDs of Figs 1–4). They were applied to the raw photometry within circular areas of radius 100 arcmin. Because the sample clusters show detached evolutionary sequences in the CMDs, we defined separate filters for each one.

For each cluster, we built profiles (Figs 9–12) corresponding to total (MS + PMS or probable-PMS) and partial (MS and PMS or probable-PMS) photometry filtered by colour and magnitudes (Section 3). Positions of projected and surrounding objects found in catalogues available in the Vizier data base – Wolf–Rayet stars (van der Hucht 2001), supernova remnants (Green 2009), dark nebulae (Dutra & Bica 2002), Herbig–Haro objects (Reipurth 1999), bright-rimmed clouds (Sugitani, Fukui & Ogura 1991) and other clusters (Dias et al. 2002; Kharchenko et al. 2013) – were superimposed on the RDPs.

We also defined a radial limit (r_{RDP}) for each cluster as the projected distance from the cluster centre where the profile and the background are indistinguishable (Table 4). Such r_{RDP} may be the intrinsic extents of the clusters (Bonatto & Bica 2007).

Using concentric annuli and the corresponding radial distance of the most populated position within each annulus, we built stellar

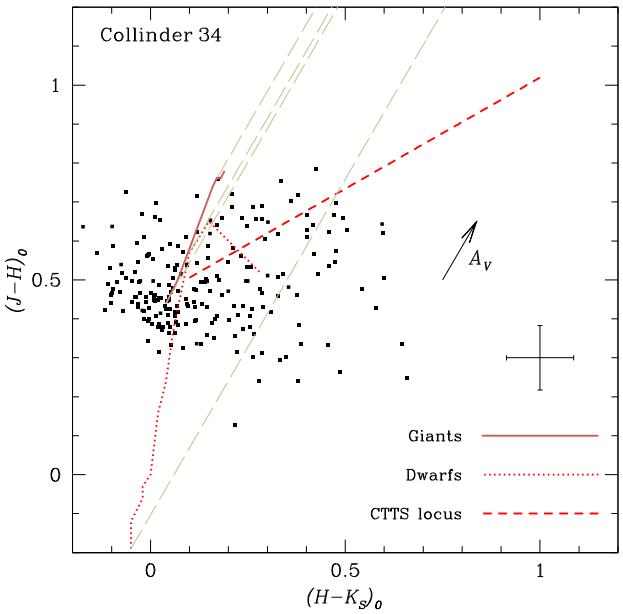

Figure 5. Collinder 34: 2MASS extinction-corrected 2CD of the probable PMS stars. Mean uncertainties are represented by the error bars. Solid line is the sequence of giants, dotted line is the sequence of dwarfs, and short-dashed line is the CTTSs locus. The arrow indicates the reddening vector for $A_V = 1.51$ mag. The long-dashed lines encompass a strip area parallel to the reddening vector. The stars with colours outside and to the right of the strip area have infrared excess emission.

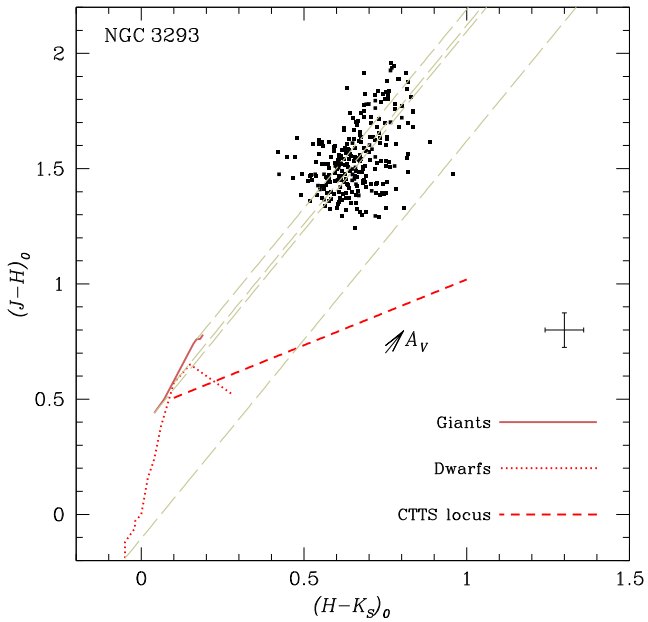

Figure 6. NGC 3293: same as Fig. 5. The arrow indicates the reddening vector for $A_V = 0.96$ mag.

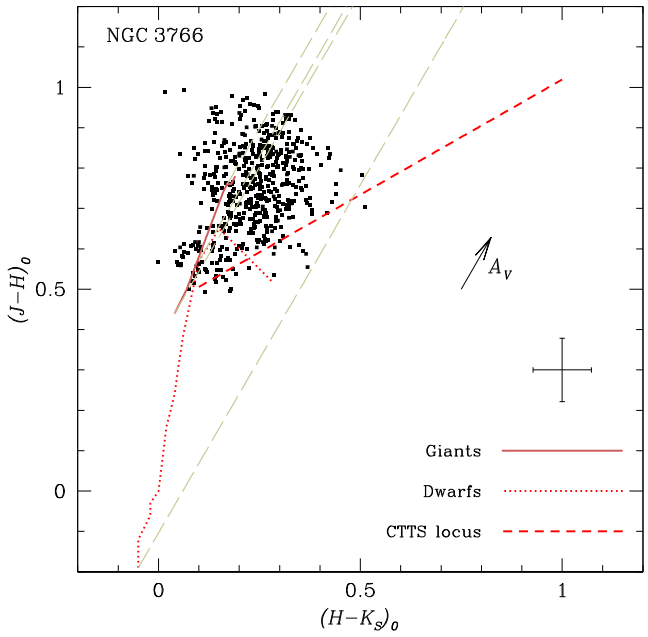

Figure 7. NGC 3766: same as Fig. 5. The arrow indicates the reddening vector for $A_V = 1.28$ mag.

RDPs for the four clusters. Since the PMS profiles are not matched by isothermal sphere models, we have chosen to fit only the MS profiles, except for Collinder 34 that has very low density of MS stars. Thus, structural parameters (Table 5) for NGC 3293, NGC 3766 and NGC 6231 were estimated by fitting their MS RDPs with a non-linear least-squares routine to a King-like (2-parameter) model given by

$$\Omega(r) = \Omega_{\rm bg} + \frac{\Omega_0}{1 + (r/r_{\rm c})^2}, \quad (1)$$

where Ω_0 is the central surface density, $r_{\rm c}$ is the core radius and $\Omega_{\rm bg}$ is the background density measured in a surrounding annulus

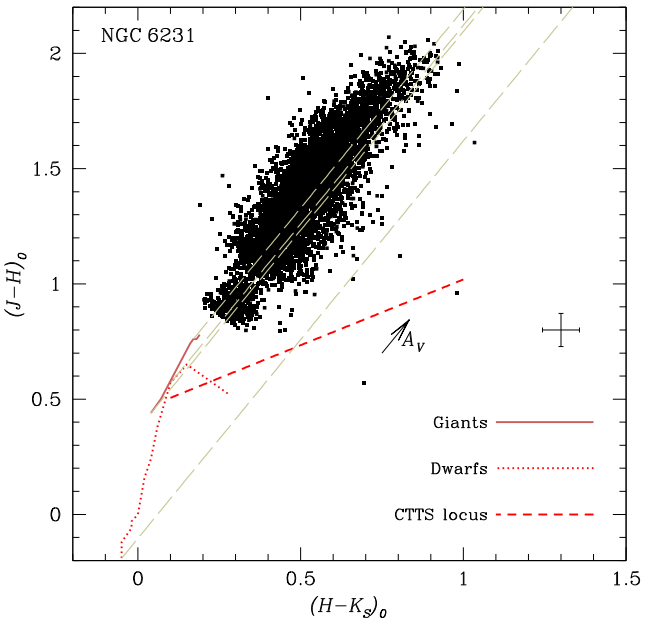

Figure 8. NGC6231: same as Fig. 5. The arrow indicates the reddening vector for $A_V = 1.44$ mag.

($80 \leq r \leq 100$ arcmin) and kept constant. The best fittings have a relatively small amount of scatter around the profile, so that the root-mean-square errors are about 2 (Table 5).

5 DISCUSSION

A comparison of the MS structural parameters obtained in this work (Table 5) with those available in the literature (Table 6) reveals similarity within uncertainties for NGC 3293 and NGC 3766. The core radius of NGC 6231 is smaller than that reported in the literature, but its MS profile represents well the core and the extension structures (Fig. 12).

Notably, each cluster in this work features a detached reddened ensemble of stars in its CMDs (Section 3) with colour gaps $\Delta(J - K_S)$ in the range 0.25–1.5 mag (Table 7). In addition, the density profiles of MS and PMS do not match each other in shape nor in extension (Figs 9–12). We analyse whether these particularities are connected to a second generation of PMS stars distributed like a halo. We emphasize that the present field star decontamination allows us to access the PMS population.

Sequential star formation may be triggered by stellar winds of massive stars or supernovae explosions. Two mechanisms were proposed to explain this process: collect-and-collapse (Elmegreen & Lada 1977) and radiation-driven implosions (Sandford, Whitaker & Klein 1982). Both may operate simultaneously in a star-forming region, but the former is an important mechanism of massive star formation because the expanding H II region sweeps out the cloud collecting material as a snowball (Zavagno et al. 2006).

Signposts of collect-and-collapse and radiation-driven implosions remain for a while. Cometary globules such as CG7S (Lefloch & Lazareff 1995), and bright-rimmed clouds such as BRC 14 (Loren & Wootten 1978), both in the complex of the Heart and Soul nebulae (that embeds Collinder 34), may be characteristic of radiation-driven implosions and collect-and-collapse, respectively.

Such substructures, further neighbouring and projected objects in the area of the sample clusters are shown in Figs 13–16 with

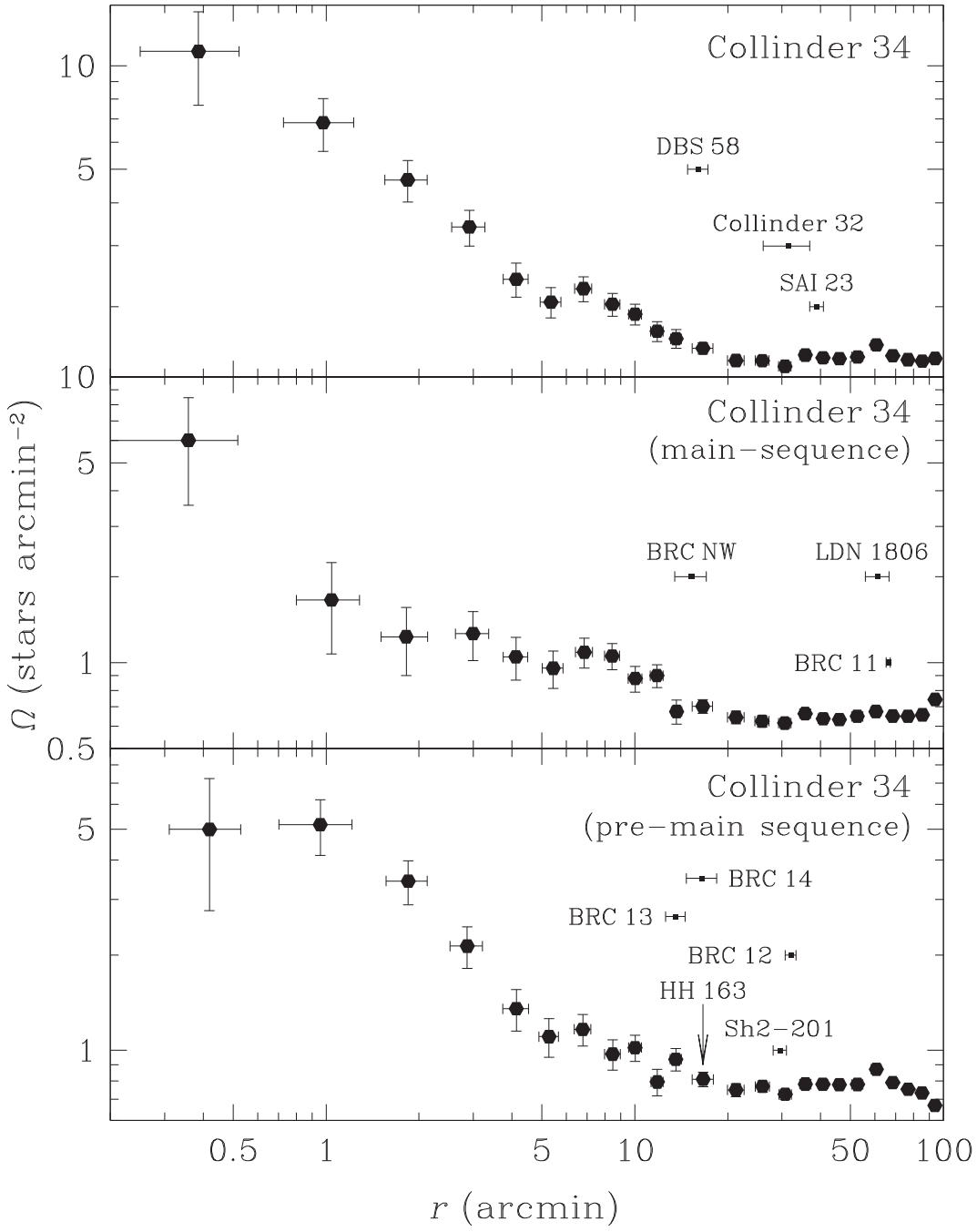

Figure 9. Collinder 34: stellar RDPs built with stars filtered by colour and magnitude (Fig. 1). Top panel: total profile (MS + PMS). Middle panel: MS profile. Bottom panel: PMS profile.

Digitized Sky Survey 2 (DSS2) *R*-band images generated by *SkyView* (McGlynn et al. 1996).

In the following, we carry out individual analyses of each cluster.

5.1 Collinder 34

Collinder 34 (Fig. 13) is part of the complex of the Heart (Sh2-190) and Soul (Sh2-199) nebulae, a star-forming region ionized by the Cas OB6 association.

Originally catalogued by Collinder (1931) at the B1900 coordinates $\alpha = 02^{\rm h}43^{\rm m}30^{\rm s}$ and $\delta = +60^{\circ}01'00''$, it was recently identified as SAI 24 (Glushkova et al. 2010). Actually, Collinder 34, together with Collinder 32 (also known as the IC 1848 cluster), is inserted in a hierarchical structure of the Collinder 33 association.

Collinder 34 is located inside a bubble in the 'baby's head" of the Sh2-199 nebula, centred in the O-type star HD 18326. It is surrounded by some infrared clusters – embedded in Sh2-201, BRC 13 and BRC 14 (Chauhan et al. 2011) – together with the small optically visible cluster BDS 58 (Bica et al. 2003).

Among the clusters in the present study, Collinder 34 has the narrowest colour gap between MS and PMS (Fig. 1), $\Delta(J - K_S) \sim 0.25$ mag. Its PMS population shows some dispersion in the 2CD (Fig. 5) and a small near-IR excess, typically

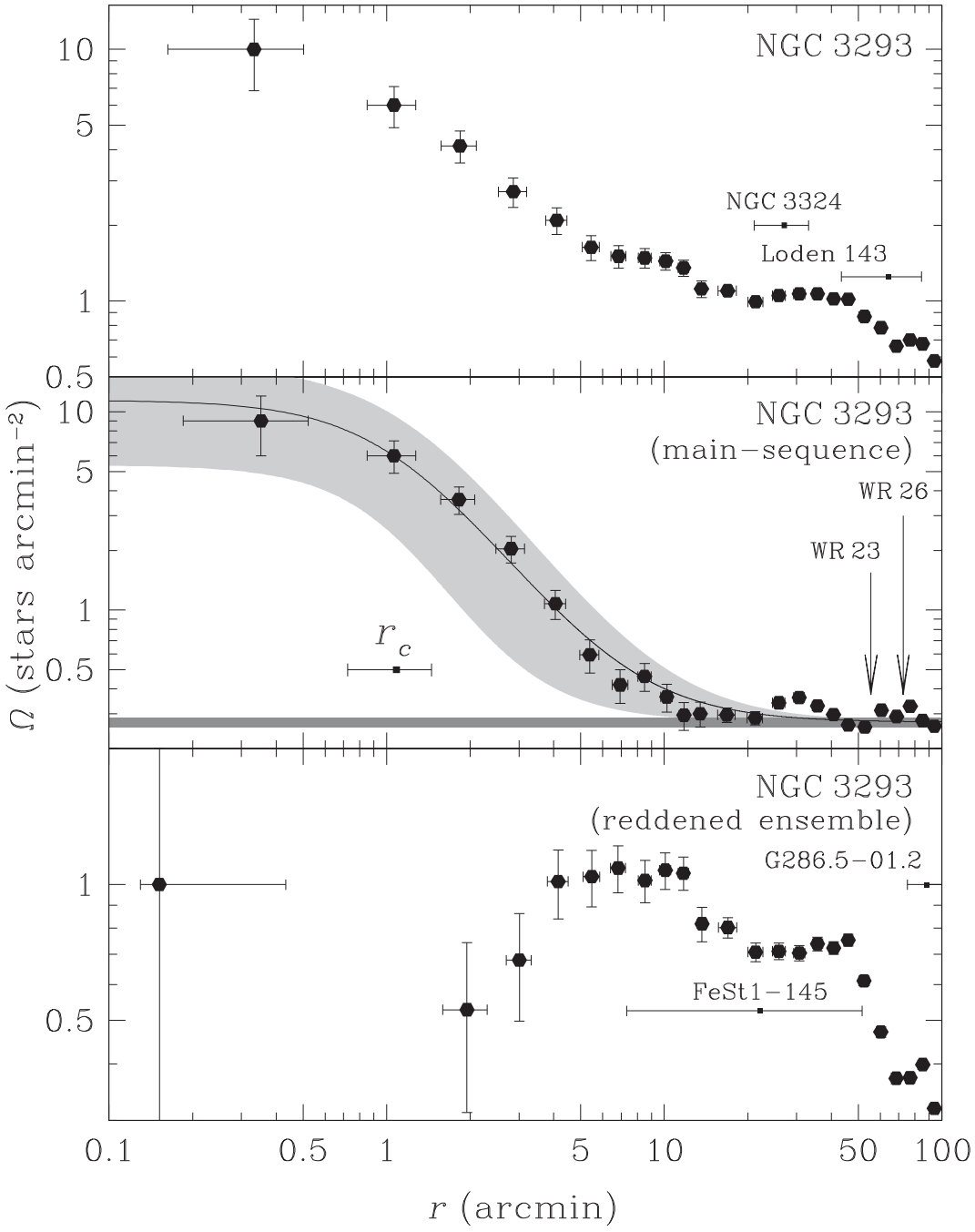

Figure 10. NGC 3293: same as Fig. 9. The fitted King-like model (equation 1) is shown as a solid line in the middle panel. The core radii (r_c) are indicated and the 3σ background stellar levels (Table 5) are represented by the narrow horizontal stripes and 1σ fit uncertainty, by the shaded regions along the fits. The positions of nearby projected objects are indicated.

associated with optically thin dust circumstellar discs featured by Weak-lined T Tauri stars (WTTSs). This is consistent with the location of the bulk of the PMS in a region limited by $(J-H)_0 \lesssim 0.5$ and $(H-K_S)_0 \lesssim 0.5$ (Meyer et al. 1997). In addition, a few points are located in $(H-K_S)_0 > 0.5$, a region usually occupied by Herbig Ae/Be stars (Hernández et al. 2005).

Stellar RDPs of Collinder 34 (Fig. 9) show a structure dominated by the PMS with its MS stars concentrated in the core. The MS profile presents an excess near the centre that cannot be interpreted as core collapse in such a young cluster. This may be characteristic of primordial mass segregation caused by competitive accretion that preferentially forms massive stars in the deepest part of the cluster potential well (Bonnell et al. 2001).

5.2 NGC 3293

Projected close to the η Carinae nebula, the star cluster NGC 3293 (Fig. 14) forms an interacting pair with NGC 3324 (de la Fuente Marcos & de la Fuente Marcos 2009; de la Fuente Marcos & de la Fuente Marcos 2010).

The sequences of NGC 3293 are separated in the decontaminated CMDs (Fig. 2) by a gap of $\Delta(J-K_S) \sim 1.5$ mag, with a heavily

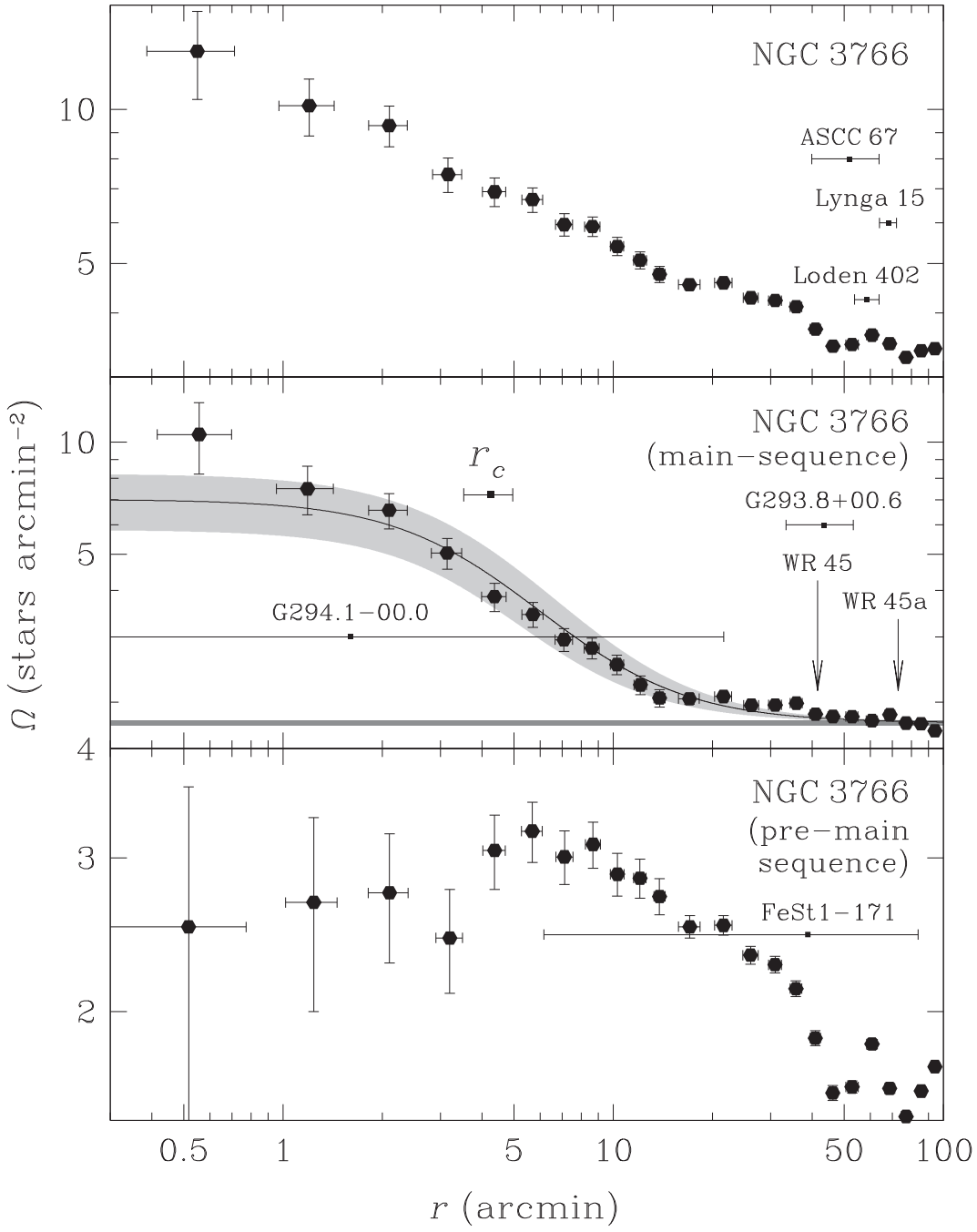

Figure 11. NGC 3766: same as Fig. 10.

reddened ensemble of stars. While, its RDPs (Fig. 10) show a centrally concentrated structure of MS stars well fitted by equation (1) (Table 5) with the reddened ensemble surrounding the core, like a halo.

An inspection of the 2CD (Fig. 6) suggests that a fraction of these reddened stars might be background dwarfs and giants that were not removed by the decontamination procedure (Section 2). Apparently, any nearby area was not adequate to model the field in detail. Anyway, the bulk of the reddened ensemble is outside the strip of dwarfs and giants, and might be formed by T Tauri stars with an absorption of $A_V \sim 3.5$ mag.

5.3 NGC 3766

The cluster NGC 3766 (Fig. 15) in the Carina complex includes the supernova remnant G294.1-00.0 (Green 2009) and at least 16 classical Be stars (McSwain, Huang & Gies 2009).

Decontaminated CMDs of NGC 3766 (Fig. 3) show a colour gap of $\Delta(J - K_S) \sim 0.5$ mag separating a broad MS and an elongated PMS. The shock wave of the supernova G294.1-00.0 might have removed the circumstellar disc of part of the PMS stars causing that elongation. In fact, an examination of the 2CD (Fig. 7) reveals a PMS with little or no near-IR excess, consistent with discless T Tauri stars.

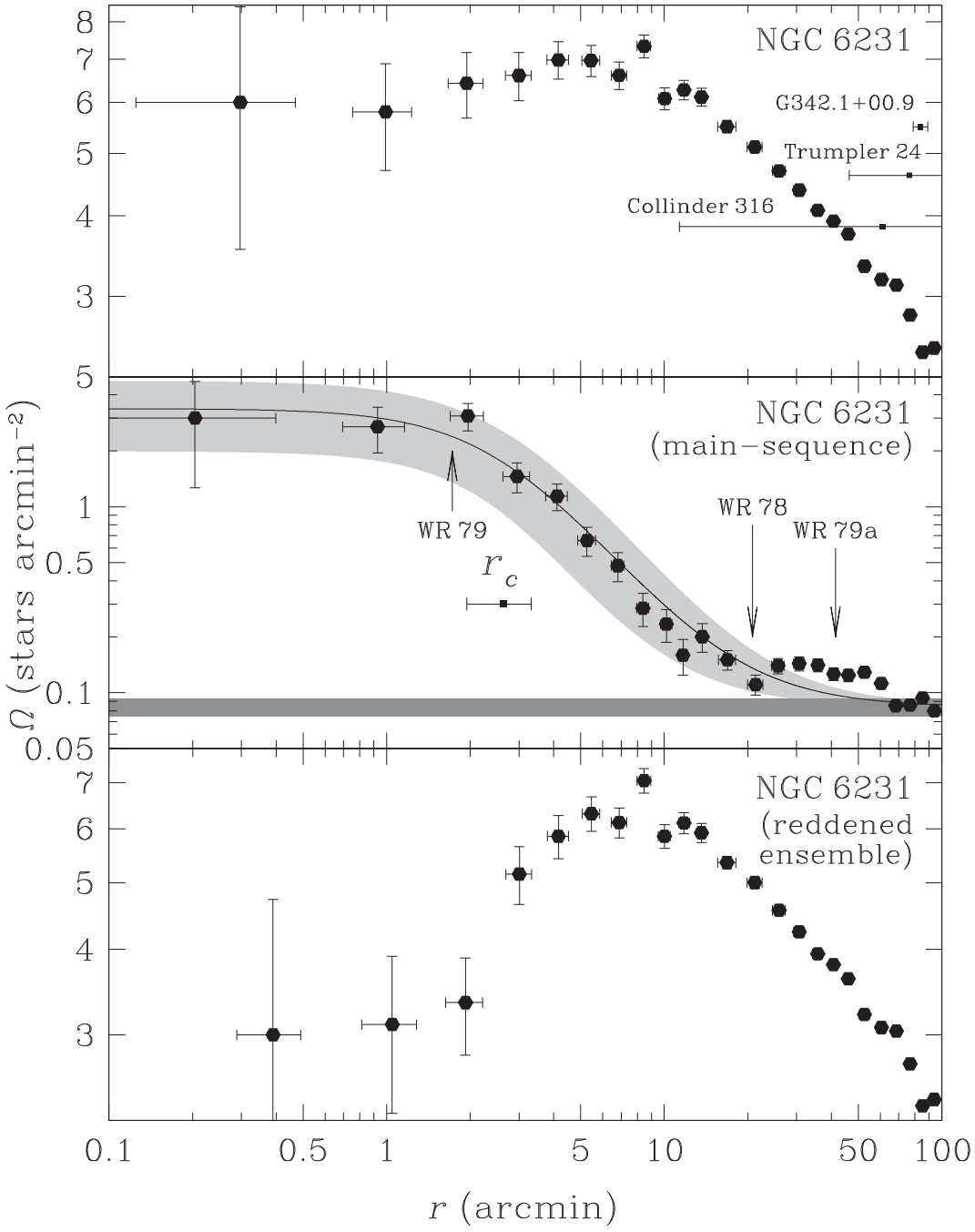

Figure 12. NGC 6231: same as Fig. 10.

Table 5. Structural parameters obtained by fitting equation (1) to the MS stellar RDPs. By columns: (1) star cluster identification; (2) background stellar density; (3) central stellar density; (4) angular core radius; (5) linear core radius; (6) root-mean-square error.

Cluster	Ω_{bg} (stars/arcmin^2)	Ω_0 (stars/arcmin^2)	r_c (arcmin)	R_c (pc)	E_{rms}
(1)	(2)	(4)	(4)	(5)	(6)
NGC 3293	0.27 ± 0.01	11.18 ± 6.06	1.09 ± 0.36	0.9 ± 0.3	2.14
NGC 3766	1.76 ± 0.01	5.26 ± 1.21	4.24 ± 0.72	2.5 ± 0.4	1.88
NGC 6231	0.08 ± 0.01	3.29 ± 1.39	2.63 ± 0.68	1.4 ± 0.4	2.20

Table 6. Cluster parameters from the literature: Dias et al. 2002 (D2002); Piskunov et a. 2007 (P2007); Bukowiecki et al. 2011 (B2011); and Kharchenko et al. 2013 (K2013). By columns: (1) star cluster identification; (2) Heliocentric distance; (3) Galactocentric distance; (4) core radius; (5) tidal radius; (6) total stellar mass; (7) age; (8) reference.

Cluster	$d_{\odot}$ (pc)	d_{GC} (pc)	R_c (pc)	R_t (pc)	M ($M_{\odot}$)	Age log(Age)	Ref.
(1)	(2)	(3)	(4)	(5)	(6)	(7)	(8)
NGC 3293	2327	–	–	–	–	7.014	D2002
	2441	–	1.30 ± 0.16	8.69 ± 1.04	–	6.75	K2013
NGC 3766	2218	–	–	–	–	7.32	D2002
	1745	–	1.3 ± 0.7	6.9 ± 1.4	2149 ± 259	7.52	P2007
	1685	–	0.91 ± 0.13	11.19 ± 1.76	–	7.95	K2013
NGC 6231	1243	–	–	–	–	6.843	D2002
	1393	–	6.84 ± 0.66	13.43 ± 0.70	–	7.05	K2013

Table 7. Star cluster RDPs diagnostic. By columns: (1) star cluster identification; (2) MS RDP morphology; (3) PMS RDP morphology; (4) extended RDP; (5) RDP with central excess; (6) $(J-K_S)$ gap between MS and PMS.

Cluster	RDP_{MS}	RDP_{PMS}	RDP_{ext}	RDP_{exc}	$\Delta(J-K_S)$
(1)	(2)	(3)	(4)	(5)	(6)
Collinder 34	non-King	King-like	no	yes	0.25
NGC 3293	King-like	non-King	yes	no	1.5
NGC 3766	King-like	non-King	yes	yes	0.5
NGC 6231	King-like	non-King	yes	no	1.0

Regarding the cluster structure, the stellar RDPs of NGC 3766 (Fig. 11) have a well fitted King-like profile of MS stars (Table 5) in a centrally concentrated structure with excess near the centre, similar to Collinder 34. In addition, its PMS stars surround the MS core, suggesting a halo.

5.4 NGC 6231

The cluster NGC 6231 (Fig. 16), at the core of the Sco OB1 association (Perry et al. 1990), is rich in early-type stars (at least 150)

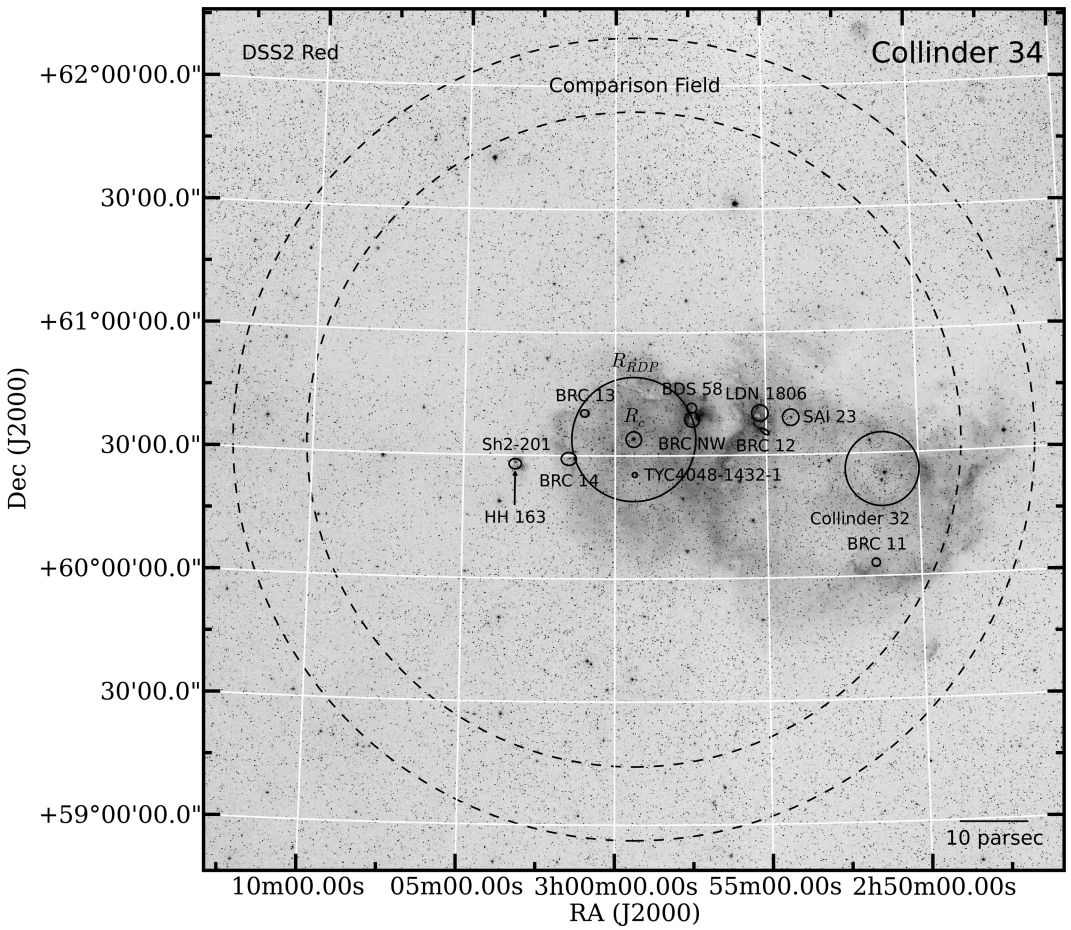

Figure 13. Collinder 34: DSS2 *R*-band image including projected and neighbouring objects embedded in the IC 1848 nebula. R_c from the total profile fitting (Table 5), R_{RDP} and annular field comparison area are also shown.

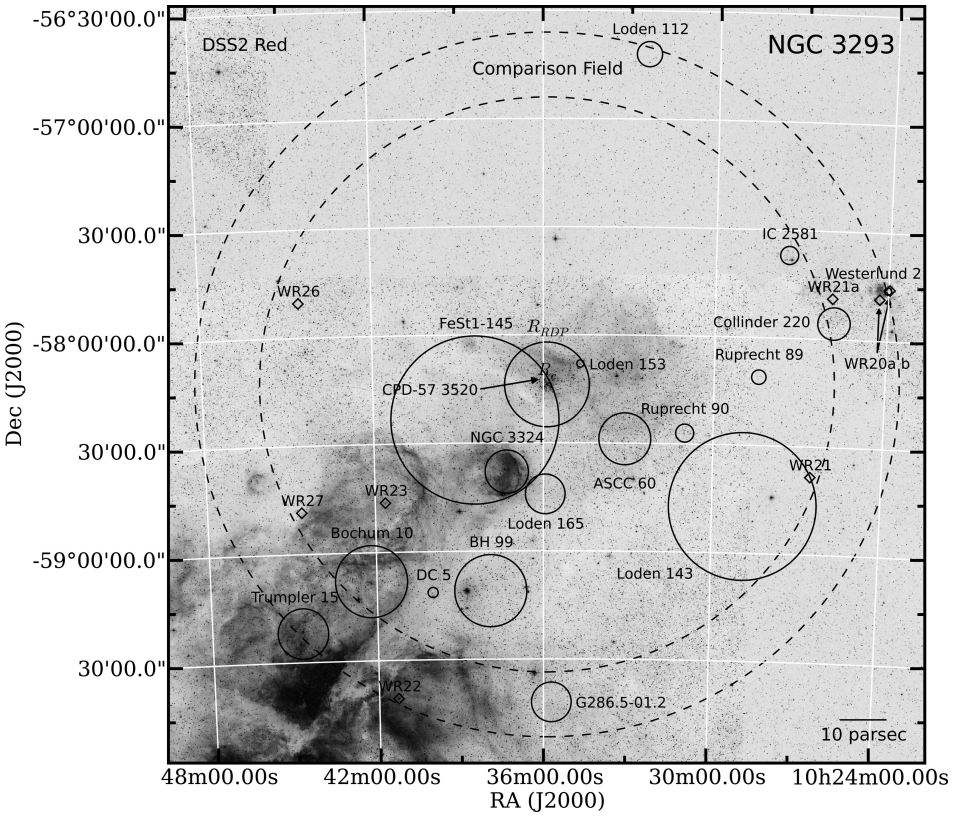

Figure 14. NGC 3293: same as Fig. 13. R_c from the MS profile fitting (Table 5).

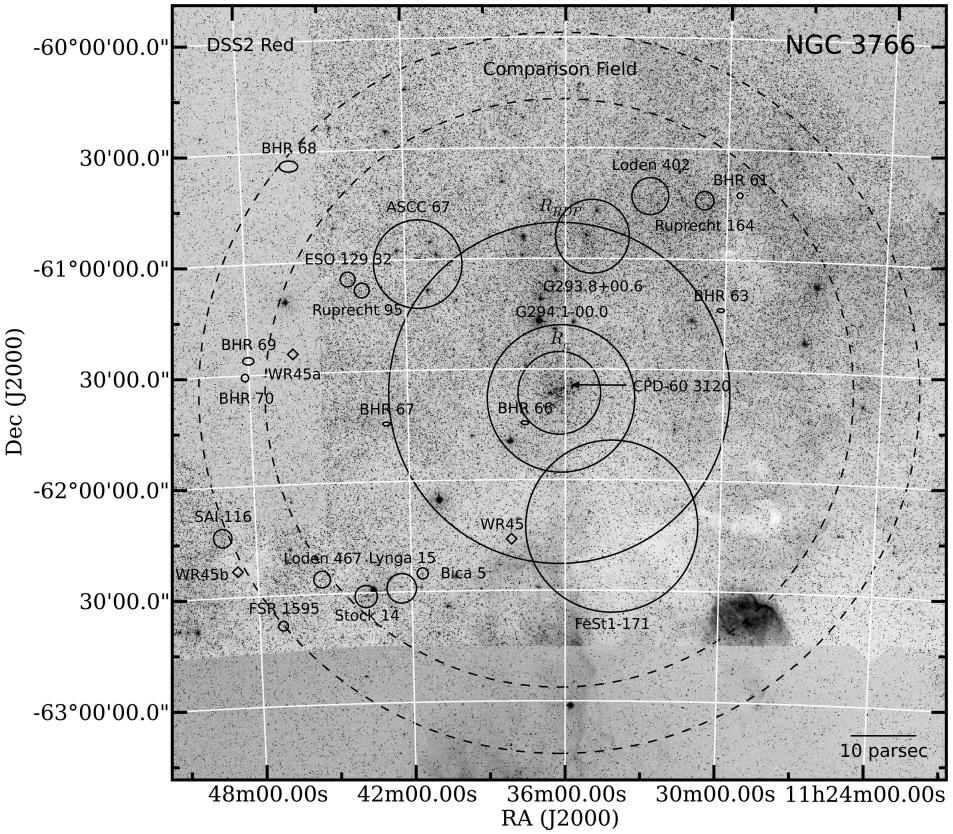

Figure 15. NGC 3766: same as Fig. 13. R_c from the total profile fitting (Table 5).

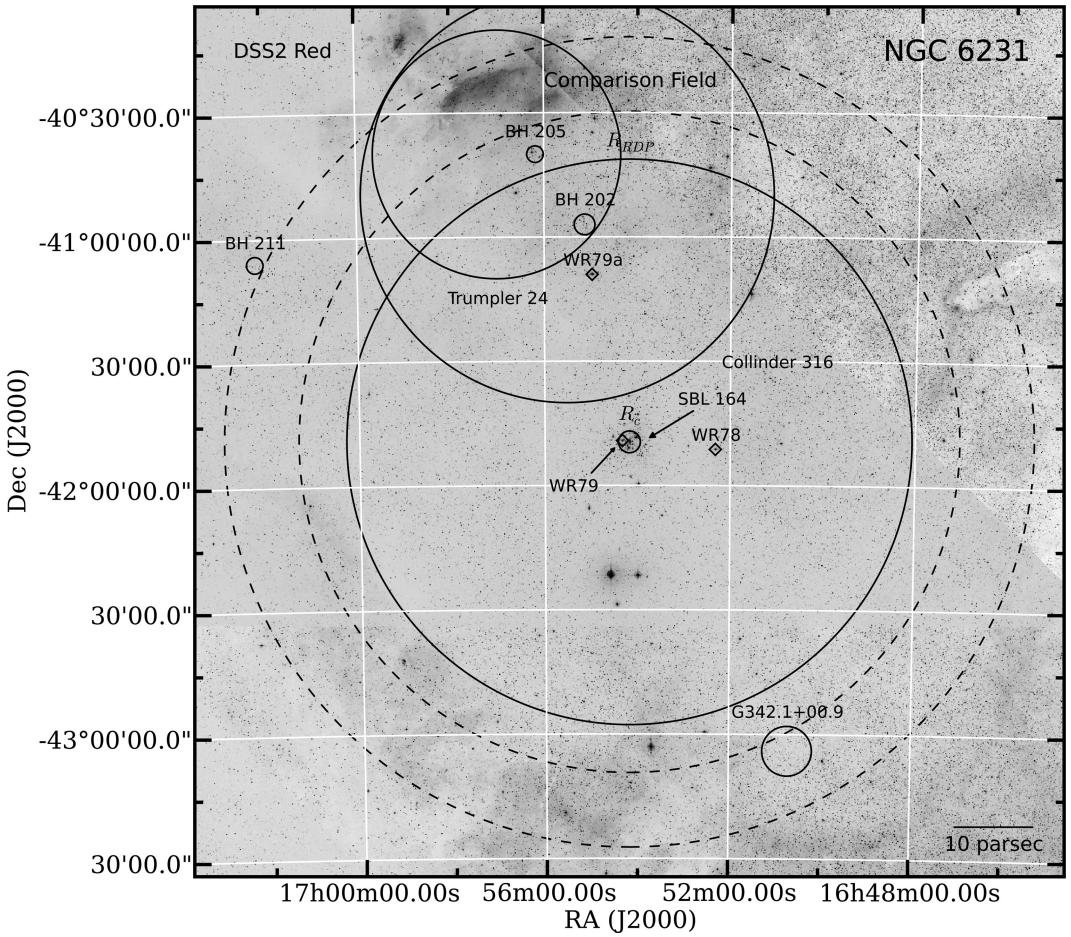

Figure 16. NGC 6231: same as Fig. 13. R_c from the MS profile fitting (Table 5).

and more than half of its OB stars are members of binary systems (Raboud 1996; Sana et al. 2008).

NGC 6231 is inside a large bubble in the Gum 55 H II region. Stellar winds of massive stars, like WR 79 (van der Hucht 2001), or past supernovae explosions might have depleted the central area of the cloud resulting in a low differential reddening and a deficit of Hα emission in the PMS stars (Sung, Bessell & Lee 1998).

Decontaminated CMDs of NGC 6231 (Fig. 4) show a narrow MS separated from a heavily reddened ensemble of stars by a wide colour gap of $\Delta(J - K_S) \sim 1.0$ mag, like that of NGC 3293 (Section 5.2).

The 2CD of NGC 6231 (Fig. 8) shows that the reddened ensemble is placed along a broad-band with a high absorption of $A_V \sim 3.5$ mag for the bulk. Furthermore, similar to NGC 3293 (Section 5.2), background dwarfs and giants seem to have survived to decontamination.

Finally, the stellar MS RDP of NGC 6231 (Fig. 12) is well fitted by equation (1) (Table 5). Such profile matches that by Sung, Sana & Bessel (2013) which extents to 20 arcmin for high-mass stars and shows an extension in $20 < r < 60$ arcmin.

5.5 Diagnostic diagrams

In order to compare the derived cluster parameters – radial limit, age, Galactocentric distance and mass – of the present sample with those of other clusters, we built diagnostic diagrams (Fig. 17) for a selected sample of young objects within the age range 1–14 Myr. They are: NGC 4755 (Bonatto et al. 2006b); NGC 6611 (Bonatto, Santos & Bica 2006a); Bochum 1 and NGC 6823 (Bica, Bonatto & Dutra 2008); NGC 2244 and NGC 2239 (Bonatto & Bica 2009); Collinder 197 and vdB 92 (Bonatto & Bica 2010); and Trumpler 37 (Saurin et al. 2012).

The radius time evolution of the clusters seems to be constrained by the Galactocentric distance and mass, as seen in Fig. 17, panels (a), (b) and (c). The more massive clusters NGC 3766 and NGC 6231 appear to keep most of their stars despite the relatively smaller Galactocentric distance. They have comparable radii to those of Bochum 1 and Trumpler 37, systems that seem to be evolving to OB associations. On the other hand, Collinder 34 and NGC 3293 occupy intermediate positions in the diagrams, mixed to the ordinary embedded clusters. Our sample is inserted into a scale of early evolving star clusters tending to dissolution, as expected for most of the embedded clusters (Lada & Lada 2003).

6 CONCLUDING REMARKS

We have studied four young star clusters and found CMDs with detached PMS from the MS at least for two objects. Colour gaps between these evolutionary sequences were revealed by field star decontamination – 0.25 mag for Collinder 34, and 0.5 mag for NGC 3766. This might be evidence of sequential star formation.

On the other hand, the clusters NGC 3293 and NGC 6231 have wider colour gaps, 1.5 and 1.0 mag, respectively. An inspection of their 2CDs suggests that those heavily reddened ensembles appear

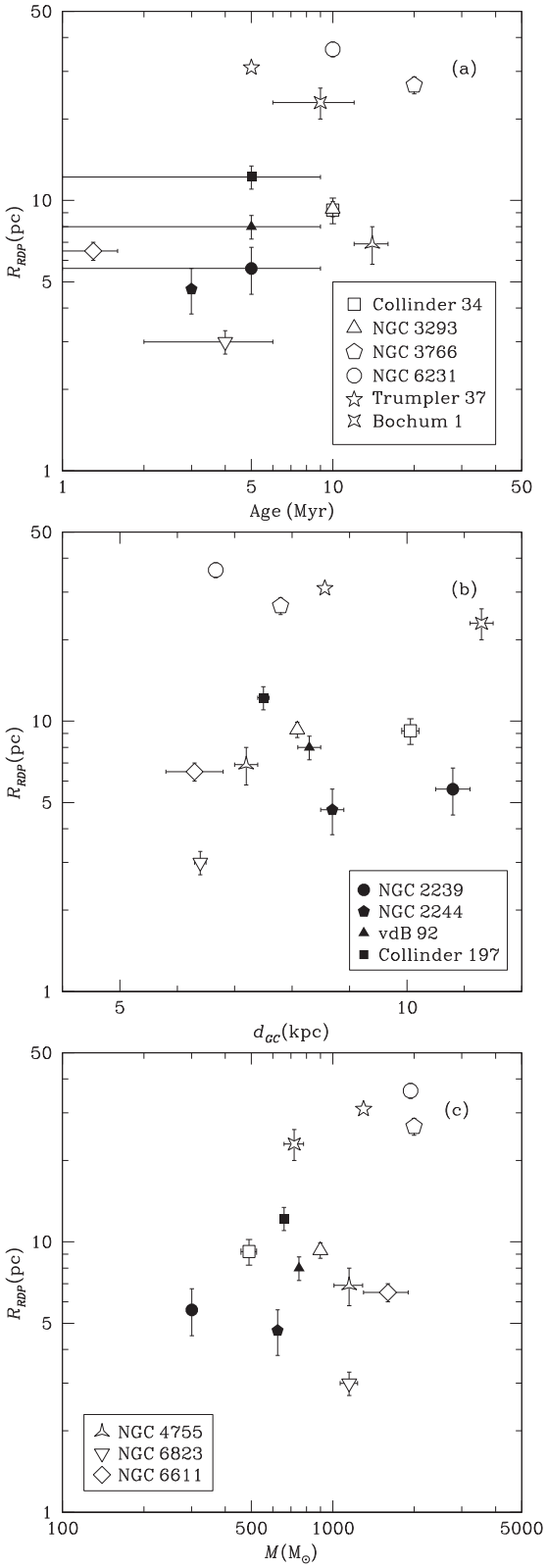

Figure 17. Diagnostic diagrams comparing cluster parameters. Some error bars are smaller than the symbols.

to be contaminated by residual background dwarfs and giants of the field. Anyway, the bulk of those ensembles might consist of very reddened PMS stars.

Spatial structures of the sequences of each cluster were examined by means of stellar RDPs revealing that the detached sequences are distributed in different ways for each cluster. The MS profiles of NGC 3293, NGC 3766 and NGC 6231 have been fitted by a King-like model yielding similar structural parameters as compared to the literature. Furthermore, the RDPs of Collinder 34 and NGC 3766 present central excesses that may represent primordial mass segregation.

Finally, this study suggests that reddened haloes of PMS stars as formed from the parental cloud may still be present after 5–20 Myr.

ACKNOWLEDGEMENTS

We acknowledge support from the Brazilian Institution CNPq. We thank an anonymous referee for constructive comments and suggestions. This research has made use of the WEBDA data base, operated at the Department of Theoretical Physics and Astrophysics of the Masaryk University. We acknowledge the use of NASA's *SkyView* facility (http://skyview.gsfc.nasa.gov) located at NASA Goddard Space Flight Center. This research has made use of the VizieR catalogue access tool, CDS, Strasbourg, France. This research has made use of the SIMBAD data base, operated at CDS, Strasbourg, France. This publication makes use of data products from the Two Micron All Sky Survey, which is a joint project of the University of Massachusetts and the Infrared Processing and Analysis Center/California Institute of Technology, funded by the National Aeronautics and Space Administration and the National Science Foundation.

REFERENCES

Bica E., Dutra C. M., Soares J., Barbuy B., 2003, A&A, 404, 223
Bica E., Bonatto C., Dutra C. M., 2008, A&A, 489, 1129
Bonatto C., Bica E., 2007, MNRAS, 377, 1301
Bonatto C., Bica E., 2009, MNRAS, 394, 2127
Bonatto C., Bica E., 2010, A&A, 516, 81
Bonatto C., Santos J. F. C., Jr., Bica E., 2006a, A&A, 445, 567
Bonatto C., Bica E., Ortolani S., Barbuy B., 2006b, A&A, 453, 121
Bonatto C., Bica E., Lima E. F., 2012a, MNRAS, 420, 352
Bonatto C., Bica E., Lima E. F., 2012b, MNRAS, 540, 137
Bonnell I. A., Bate M. R., Clarke C. J., Pringle J. E., 2001, MNRAS, 323, 785
Bukowiecki L., Maciejewski G., Konorski P., Strobel A., 2011, Acta. Astron., 61, 231
Carpenter J. M., 2001, AJ, 121, 2851
Chauhan N., Pandey A. K., Ogura K., Jose J., Ojha D. K., Samal M. R., Mito H., 2011, MNRAS, 415, 1202
Collinder P., 1931, Academical Dissertation, Philosophical Faculty of Lund
Cutri R. M. et al., 2003, 2MASS All-Sky Catalog of Point Sources, VizieR Online Data Catalog, 2246
de la Fuente Marcos R., de la Fuente Marcos C., 2009, ApJ, 700, 436
de la Fuente Marcos R., de la Fuente Marcos C., 2010, ApJ, 719, 104
Dias W. S., Alessi B. S., Moitinho A., Lepine J. R. D., 2002, A&A, 389, 871
Dutra C. M., Bica E., 2002, A&A, 383, 631
Dutra C. M., Santiago B. X., Bica E., 2002, A&A, 381, 219
Elmegreen B. G., Lada C. J., 1977, ApJ, 214, 725
Furlan E. et al., 2009, ApJ, 703, 1964
Glushkova E. V., Koposov S. E., Zolotukhin I. Yu., Beletsky Yu. V., Vlasov A. D., Leonova S. I., 2010, Astron. Lett., 36, 75
Green D. A., 2009, Bull. Astron. Soc. India, 37, 45

Hernández J., Calvet N., Hartmann L., Briceño C., Sicilia-Aguilar A., Berlind P., 2005, AJ, 129, 586
Hillenbrand L. A., 1997, AJ, 113, 1733
Kenyon S. J., Hartmann L., 1995, ApJS, 101, 117
Kharchenko N. V., Piskunov A. E., Schilbach E., Röser S., Scholz R.-D., 2013, A&A, 558, 53
King I., 1962, AJ, 67, 471
Kroupa P., 2001, MNRAS, 322, 231
Lada C. J., Lada E. A., 2003, ARA&A, 41, 57
Lefloch B., Lazareff B., 1995, A&A, 301, 522
Loren R. B., Wootten H. A., 1978, ApJ, 225, 81
McGlynn T., Scollick K., White N., 1996, in McLean B. J., Golombek D. A., Hayes J. J. E., Payne H. E., eds, Proc. IAU Symp. 179, New Horizons from Multi-Wavelength Sky Surveys. Kluwer Academic Publishers, Dordrecht, p. 465
McSwain M. V., Huang W., Gies D. R., 2009, ApJ, 700, 1216
Marigo P., Girardi L., Bressan A., Groenewegen M. A. T., Silva L., Granato G. L., 2008, A&A, 482, 883
Meyer M. R., Calvet N., Hillenbrand L. A., 1997, AJ, 114, 288
Ochsenbein F., Bauer P., Marcout J., 2000, A&AS, 143, 23
Perry C. L., Hill G., Younger P. F., Barnes J. V., 1990, A&AS, 86, 415
Piskunov A. E., Schilbach E., Kharchenko N. V., Röser S., Scholz R.-D., 2007, A&A, 468, 151
Raboud D., 1996, A&A, 315, 384
Reid M. J. et al., 2009, ApJ, 700, 137
Reipurth B., 1999, A General Catalogue of Herbig–Haro Objects, 2nd edn Available at: http://casa.colorado.edu/hhcat. Accessed on January 21, 2015
Sana H., Gosset E., Nazé Y., Rauw G., Linder N., 2008, MNRAS, 386, 447
Sandford M. T., II, Whitaker R. W., Klein R. I., 1982, ApJ, 260, 183
Saurin T. A., Bica E., Bonatto C., 2010, MNRAS, 407, 133
Saurin T. A., Bica E., Bonatto C., 2012, MNRAS, 421, 3206
Schmidt-Kaler T., 1982, Landolt-Börnstein, New Series, Group VI, Vol. 2b. Springer-Verlag, Berlin, p. 1
Siess L., Dufour E., Forestini M., 2000, A&A, 358, 593
Skrutskie M. F. et al., 2006, AJ, 131, 1163
Sugitani K., Fukui Y., Ogura K., 1991, ApJS, 77, 59
Sung H., Bessell M. S., Lee S.-W., 1998, AJ, 115, 734
Sung H., Sana H., Bessell M. S., 2013, AJ, 145, 37
van der Hucht K. A., 2001, New Astron. Rev., 45, 135
Wenger M. et al., 2000, A&AS, 143, 9
Zavagno A., Deharveng L., Comerón F., Brand J., Massi F., Caplan J., Russeil D., 2006, A&A, 446, 171

This paper has been typeset from a TEX/LATEX file prepared by the author.